Spontaneous coherence and the quantum Hall effect in triple-layer electron systems

C. B. Hanna and A. H. MacDonald

Department of Physics, Indiana University, Bloomington, Indiana 47405

(Received 10 January 1996)

We investigate spontaneous interlayer phase coherence and the occurrence of the quantum Hall effect in triple-layer electron systems. Our work is based on a simple tight-binding model that greatly facilitates calculations and whose accuracy is verified by comparison with recent experiments. By calculating the ground state in an unrestricted Hartree-Fock approximation and the collective-mode spectrum in a time-dependent Hartree-Fock approximation, we construct a phase diagram delimiting regions in the parameter space of the model where the integer quantum Hall effect occurs in the absence of interlayer tunneling. [S0163-1829(96)05723-2]

I. INTRODUCTION

Interactions among particles play an especially important role in two-dimensional (2D) systems in the quantum Hall (QH) regime because the kinetic energy is quenched. Kinetic energy eigenstates bunch into quantized Landau levels with macroscopic degeneracy $N_\phi = B_\perp A / \Phi_0$. (Here A is the cross-sectional area of the system, $B_\perp$ is the magnetic field strength, and $\Phi_0 = hc/e$ is the magnetic flux quantum.) The fractional QH effect (QHE),[1] which occurs when an orbitally degenerate Landau level has a fractional filling factor $\nu_T \equiv N_e / N_\phi$, where N_e is the total number of electrons, arises from strongly correlated states produced entirely by interactions.[2,3]

Interactions can play an important role even at integer values of ν_T, if at low energies the system has additional degrees of freedom. An important example occurs for an isolated 2D electron layer at $\nu_T = 1$, when the Zeeman energy is so small that the spins are not completely frozen. It turns out in this case that the ground state is completely spin polarized, and that the energy gap for charged excitations (which gives the QHE) is finite, even in the limit of vanishing Zeeman splitting. However, there is strong experimental evidence that for ν_T close, but not equal, to 1, the ground state contains a large number of flipped spins.[4] This property of the single-layer system, which was anticipated theoretically,[5–7] is best understood by recognizing that the ground state at $\nu_T = 1$ is a 2D ferromagnet with spontaneous spin polarization. 2D ferromagnets have stable finite-energy topologically charged spin-texture excitations, commonly known as skyrmions.[8] A unique aspect of these QH ferromagnets, first appreciated by Sondhi *et al.*,[6] is that their skyrmions also carry a unit electrical charge. It is the presence of these unusual charged objects with many reversed spins in their interior that is responsible for the rapid decline in the spin polarization that occurs as ν_T moves away from 1. Many aspects of the physics are very similar[9–13] when the additional degree of freedom comes from a second electron layer, rather than from the two spin states available to spin-1/2 particles. The role played by the Zeeman energy is taken over in this case by the interlayer hopping amplitude t, the broken symmetry is spontaneous interlayer phase coherence rather than spin magnetization, and a QHE can occur[14,15] at $\nu_T = 1$, even when $t = 0$. The combination of the integer QHE

and spontaneous broken symmetry in the ground state gives rise to charged order-parameter textures and other new physics.[9]

In this paper, we consider the case of triple-layer electron systems (TLES's). Our work is motivated primarily by recent progress in fabricating high-mobility electron systems, which has made it possible to study these systems experimentally.[16–18] Triple-layer systems in strong magnetic fields have been studied previously,[19] but the possibility of QHE's associated with spontaneously broken symmetries,[10] on which we focus here, was not explicitly addressed. In Sec. II of this paper, we introduce the tight-binding model that we use to describe TLES's in terms of a small number of parameters. We make some estimates of the size of the model parameters in Sec. III, and discuss some electrostatic considerations that are very important in interpreting experiments. We test our model and demonstrate the possibility of determining its parameters by comparing with some recent experiments at weak magnetic fields. In Sec. IV, we discuss unrestricted Hartree-Fock approximations (HFA's) for the ground state of TLES's in a strong magnetic field. The HF wave functions allow for the possibility of spontaneous interlayer phase coherence and are generalizations of those proposed previously[20] for double-layer systems at $\nu_T = 1$:

$$|\Psi\rangle = \prod_X^{N_\phi} (e^{i\phi_1} \hat{c}_{1X}^\dagger + e^{i\phi_2} \hat{c}_{2X}^\dagger)|0\rangle. \qquad (1.1)$$

Here X is the guiding-center label for orbital states within a Landau level in the Landau gauge, which we use throughout this paper. This many-particle wave function exhibits interlayer coherence, because all electrons occupy states that are a linear superposition of layer $j = 1$ and layer $j = 2$. When $\phi_1 = \phi_2$, Eq. (1.1) represents a full Landau level formed from the symmetric combination of isolated layer states, and is evidently the exact ground state for a system of noninteracting electrons, when tunneling between the layers is described in a tight-binding model. It turns out that it is also the exact ground state in the presence of repulsive interactions, even without tunneling, when the interactions are independent of the layer index j (i.e., in the limit that the layer separation $d \to 0$). When the interlayer Coulomb interactions are different from the intralayer interactions ($d > 0$), Eq. (1.1) is still a good variational wave function because phase

coherence guarantees good interlayer electronic correlations and thereby lowers the interlayer Coulomb interaction energy.[9] Only when the layers are widely separated does Eq. (1.1) become a poor variational wave function; eventually, it becomes much more important to have good intralayer correlations than to have good interlayer correlations. In this case, the ground state no longer has spontaneous interlayer correlations and the QHE will not generally occur at $\nu_T=1$ in the absence of interlayer tunneling. (An exception occurs when the electrostatic environment is consistent with having QHE's in which interlayer correlations play no role, for example, by having $\nu=1/3$ in each layer.) In Sec. V, we evaluate the collective-mode dispersion of a TLES in the time-dependent HF approximation (TDHFA). In the absence of interlayer tunneling, the energy in the double-layer case is independent of the global phases ϕ_j. The U(1) symmetry associated with $\phi_{12}\equiv\phi_1-\phi_2$ is broken in the ground state of the double-layer system, giving rise to a gapless Goldstone mode associated with slow spatial variations of ϕ_{12}.[10,12] The energy cost of the spatial variations of $\phi_{12}(X)$ is due to the loss of interlayer Coulomb exchange energy. We find that in triple-layer systems, two Goldstone modes occur, associated with the two independent relative phases. We use the stability of the collective modes as an indication that the HF variational wave function is still good, and use this criterion to map out the region in the model's parameter space where we expect a triple-layer integer QHE to occur with spontaneous interlayer phase coherence in the ground state. Section VI contains some brief concluding remarks. A future work will discuss charged order-parameter textures and the effect of tilted magnetic fields in triple-layer systems, using a field-theoretic approach.

II. MODEL FOR TRIPLE-LAYER SYSTEMS

Triple-layer QH systems have been realized experimentally by Shayegan and co-workers.[16–18] In order to observe the QHE, the mobility of these samples needs to be very high, which generally requires that they be remotely doped. The simplest possible theory of the triple-layer system is one that regards it as a macroscopic metal, and therefore requires that the volume between the right and left layers be an equipotential. In such a theory, the Poisson equation allows no charge in the central layer; repulsive interactions between the electrons cause them to migrate to the left and right layers. Obviously, this theory is incomplete, but its indication that electrons tend to avoid the middle layer is telling, and this tendency must be countered if true triple-layer systems are to be realized. In the TLES's grown by Shayegan's group, the middle layer is wider than the outside layers and therefore has a smaller size-quantization energy.

The Shayegan group has demonstrated[16–18] that at zero magnetic field, the partitioning of electron density between the three layers as a function of gate voltage can be accurately rendered using a three-dimensional (3D) density-functional-based independent-electron approximation. In order to describe the many-body physics of these systems, which is essential at strong magnetic fields, we require a relatively simple model for the growth-direction (z-direction) spatial degree of freedom. We proceed by generalizing the approach commonly used for double-layer 2D

electron systems. We assume that only the lowest electric subband is important in each 2D layer, and use a tight-binding description for the z-direction degree of freedom, with tunneling amplitude t between neighboring layers, and no direct tunneling between left and right layers. (Remote tunneling can be readily incorporated in the model, if the experimental situation warrants introducing this complication.) For the calculations reported here, we neglect the finite width of the subband wave functions in each layer, but these can easily be modeled if necessary in specific systems by adding form-factor corrections[21] to the effective electron-electron interaction. We assume that the subband energy in the middle layer (relative to the local electrostatic potential) differs from the subband energies in the side layers (also relative to the local electrostatic potential) by ϵ_b.

In experiments on TLES's, it is extremely useful to be able to manipulate charges in the layers with both a front (F) gate, which we take to be closest to the left layer, and a back (B) gate, which we take to be closest to the right layer. We parametrize these gate voltages in terms of neutralizing charge densities p_α ($\alpha=F,B$), by defining

$$V_{\alpha G}=\frac{4\pi e}{\epsilon_0}p_\alpha D_{\alpha G}-V_{\alpha G}^{(0)}, \qquad (2.1)$$

where $\epsilon_0\approx 13$ is the dielectric constant for GaAs and $D_{\alpha G}$ is the distance from the closest layer in the system to gate α. (For the systems fabricated by the Shayegan group, $D_{FG}\approx 0.45$ μm and $D_{BG}\approx 0.45$ mm.[22]) The last term represents an offset voltage. This model for the triple-layer system is illustrated schematically in Fig. 1.

To test the appropriateness of such a model, and to determine model parameters for the experimental system with which we will later compare our strong magnetic-field theory, we have calculated the dependence of the state of the triple-layer system on the front-gate voltage (V_{FG}). For this purpose, we have used a 2D version of the 3D local-density-functional (LDF) theory.[23] The Kohn-Sham single-particle equations separate and yield three two-dimensional free-electron bands with minima at subband energies that are determined by solving the three-site discrete Schrödinger equation for the z-direction degree of freedom. In this equation, neighboring layers are coupled by the tunneling matrix element $-t$ and the LDF site energies are given (up to a common constant term) by

$$\epsilon_1=\frac{2\pi e^2 d}{\epsilon_0}[(n_1-n_3)-(p_F-p_B)]+\mu_{xc}(n_1),$$

$$\epsilon_2=\epsilon_b+\frac{2\pi e^2 d}{\epsilon_0}n_2+\mu_{xc}(n_2),$$

$$\epsilon_3=\frac{2\pi e^2 d}{\epsilon_0}[(n_3-n_1)-(p_B-p_F)]+\mu_{xc}(n_3). \quad (2.2)$$

The "bare" middle-well on-site energy ϵ_b represents the difference in the size-quantization energy of the middle layer, relative to that of the side layers. It is negative (attractive) when the middle well is wider than the side wells. The Hartree terms are proportional to $2\pi e^2 d/\epsilon_0$. The areal densities of the left, middle, and right layers are denoted
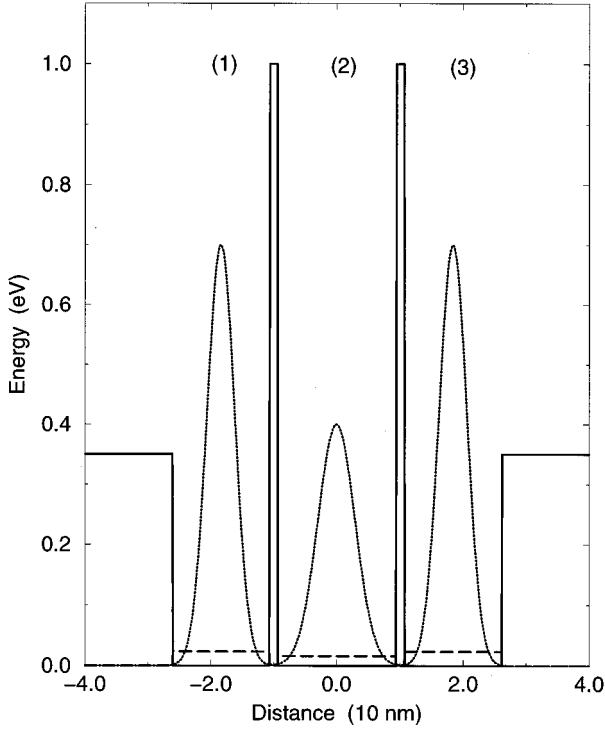
FIG. 1. Schematic illustration of the triple-layer electron system of Ref. 18. The solid lines represent the energy of the confining barriers, and the long-dashed lines are the energies of the lowest-energy quantum state for a given well. The dotted curves represent electron densities, which are peaked at midwell. Our model idealizes the electron density to be midwell δ functions.

by n_1, n_2, and n_3, respectively. The exchange contribution to the exchange-correlation potential μ_{xc} of local-density-functional theory is $\mu_x(n) = d[n\epsilon_x(n)]/dn = -e^2\sqrt{8n/\pi}/\epsilon_0$, where $\epsilon_x(n)$ is the contribution to the exchange energy per particle in a 2D electron gas of uniform density n.[23] We have not included correlation-energy contributions to μ_{xc}, but this could be added if desired. The subband energies E_λ are obtained by diagonalizing the 3×3 LDF Hamiltonian matrix. The density in layer j is given by

$$n_j = \sum_{\lambda=1}^{3} N_\lambda |z_j^{(\lambda)}|^2, \qquad (2.3)$$

where

$$N_\lambda \equiv (E_F - E_\lambda)\nu_0 \Theta(E_F - E_\lambda) \qquad (2.4)$$

is the areal-density contribution from the λth subband, $z_j^{(\lambda)}$ is the amplitude of the λth subband wave function in layer j, and $\nu_0 = m^*/\pi\hbar^2$ is the 2D electron-gas density of states ($m^* \approx 0.07 m_e$ is the band effective mass for GaAs). Equations (2.2) and (2.3) have to be solved self-consistently, with the Fermi energy chosen so that $\Sigma_\lambda N_\lambda = N_T = p_F + p_B$, consistent with overall charge neutrality.

III. MODEL PARAMETERS

Rough estimates of the size of the model parameters may be obtained from simple arguments. In the limit of infinitely strong barriers separating the layers, the size-quantization en-

ergies are $\pi^2\hbar^2/2m^*w_j^2$, where w_j is the width of the jth quantum well. For side-well widths of 15.4 nm and a middle-well width of 18.8 nm, the difference in the size-quantization energies gives $\epsilon_b \sim -8$ meV for the TLES of Shayegan and co-workers that we study here. We note that the next group of three electric subbands is higher in energy by roughly $3\pi^2\hbar^2/2m^*w^2 \sim 50$ meV, and may be neglected in studying the ground state and low-energy excitations of the TLES. The tunneling energy may be crudely estimated from a semi-classical (WKB) argument, by equating $2t/\hbar$ with the rate at which the wave-function amplitude of an electron leaks out of its well by tunneling through the confining barrier:

$$\frac{2t}{\hbar} \sim \frac{v}{2w} e^{-\kappa b} = \frac{1}{\hbar}\frac{E_0}{\pi} e^{-\kappa b}, \qquad (3.1)$$

where $v/2w$ is the frequency with which an electron of average velocity $v = \sqrt{2E_0/m^*}$ in a well of width $w \sim 17$ nm hits the side of the well, $E_0 \approx \pi^2\hbar^2/2m^*w^2 \sim 20$ meV is the energy of the confined electron, $\hbar\kappa = \sqrt{2m^*(V_0 - E_0)} \approx \sqrt{2m^*V_0}$, where[22] $V_0 \approx 1$ eV is the barrier height, and $b \approx 1.3$ nm is the width of the barrier. From this estimate, the tunneling energy $t \sim 0.5$ meV, and is thus expected to be an order of magnitude smaller than the on-site energy ϵ_b. We numerically solved the one-dimensional Schrödinger equation for the triple quantum-well potential shown in Fig. 1 in an effective-mass approximation to obtain the bound-state energies. The three lowest energies determine ϵ_b and t through Eqs. (3.5) and (3.6), and give $\epsilon_b \approx -4.7$ meV and $t \approx 0.5$ meV. We also find an energy separation of 34 meV to the next group of three electric subbands.

Electrostatic energies tend to be larger than planar kinetic energies, tunneling energies, and exchange-correlation energies. For the densities shown in Fig. 2, electrostatic energies are typically about four times larger than planar kinetic energies, about six times larger than the exchange energy, and can be on the order of 100 times larger than the tunneling energies, depending on the barrier widths. As a result, Fig. 2 can be understood qualitatively in an electrostatic approximation, where the electronic charge resides entirely in the layer with the lowest (Hartree plus ''bare'' on-site) site energy, unless two or more layers are placed in equilibrium by having the same energies. For $4\pi e^2 d p_F/\epsilon_0 \lesssim \epsilon_b < 0$, it follows that in this approximation, all electrons will occupy the right layer, and $n_3 = p_B + p_F$. With increasing p_F, charge will be added first to the middle layer, until $\epsilon_b + 4\pi e^2 d p_F/\epsilon_0 \approx 0$. As p_F is increased further, all charge is added to the left layer. These considerations provide two straightforward measurements of ϵ_b. First, at the front-gate voltage $V_3 \approx -0.3$ V where the third subband first becomes occupied, electrostatic considerations show that

$$\epsilon_b \approx -\frac{2\pi e^2 d}{\epsilon_0} N_2(V_3) \approx -4.7 \text{ meV} \qquad (3.2)$$

for $N_2(V_3) \approx 3.5 \times 10^{10}$ cm^{-2} and $d = 18.4$ nm. Second, for fixed back-gate voltage, the difference between V_3 and the value of the front-gate voltage ($V_2 \sim -0.6$ V) at which the second subband first becomes occupied also measures ϵ_b:
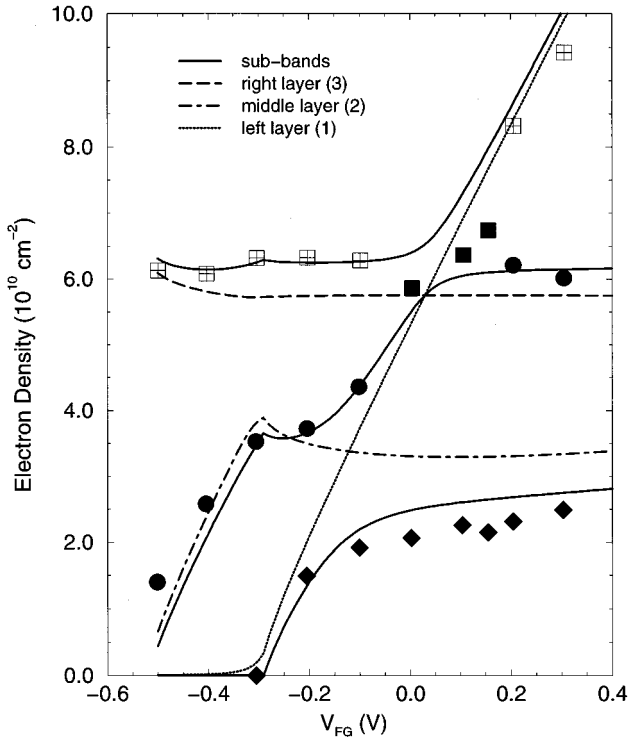
FIG. 2. Shubnikov–de Haas data taken from Ref. 18, and the subband (solid curves) and layer densities calculated from the tight-binding model described in the text.

$$\epsilon_b \approx -\frac{1}{2} \frac{ed}{D_{FG}} (V_3 - V_2)$$

$$\approx -\frac{2\pi e^2 d}{\epsilon_0} (V_3 - V_2) \frac{dN_T}{dV_{FG}} \sim -6 \quad \text{meV} \qquad (3.3)$$

for $V_3 - V_2 \sim 0.3$ V. In Eq. (3.3), we have used the fact that $1/D_{FG}$ is proportional to the front-gate capacitance per unit area, $d(-eN_T)/dV_{FG}$.

When the dependence of the chemical potential on the density in each layer is taken into account, there is a small correction to the electrostatic result. This correction is measurable, and has been exploited by Eisenstein and co-workers[24,25] in the double-layer case to measure the compressibility of the electron-gas systems within each layer. For example,[16] features occur in the charge-density distribution when the density in one of the layers is very small, which reflect the diverging (negative) compressibility in the low-density limit of an electron gas. In this picture, adding tunneling between the layers turns crossings of site energies into avoided crossings of subband energies, and smooths out cusps in the dependences of the subband densities on the electric field.

For double-layer systems, the hopping parameter t is simply related to the subband energy separation when the gate voltage is adjusted so that the two layers have equal density: $2t = E_2 - E_1$. This simple relationship is very helpful in characterizing experimental systems. It is worth remarking that a similar simple relationship exists for triple-layer systems. When $p_F = p_B$, inversion symmetry guarantees that $n_1 = n_3$ and $\epsilon_1 = \epsilon_3$. The Hamiltonian matrix can be readily diagonalized for this case with the result:

$$E_1 = \frac{\epsilon_1 + \epsilon_2}{2} - \sqrt{\left(\frac{\epsilon_1 - \epsilon_2}{2}\right)^2 + 2t^2},$$

$$E_2 = \epsilon_1,$$

$$E_3 = \frac{\epsilon_1 + \epsilon_2}{2} + \sqrt{\left(\frac{\epsilon_1 - \epsilon_2}{2}\right)^2 + 2t^2}. \qquad (3.4)$$

The subband energies E_λ can be determined up to an overall constant by the sublayer occupancies N_λ, which are obtained from the Shubnikov–de Haas (SdH) experiments, using Eq. (2.4). Equation (3.4) can be solved to express $\epsilon_2 - \epsilon_1$ and t in terms of the two independent subband energy differences. We find that

$$\epsilon_2 - \epsilon_1 = E_3 - 2E_2 + E_1, \qquad (3.5)$$

and that

$$t = \sqrt{\frac{(E_3 - E_2)(E_2 - E_1)}{2}}. \qquad (3.6)$$

Since it is clear from Fig. 2 that, for the experimental system, $E_3 - E_2 > E_2 - E_1$ when inversion symmetry is established, we see immediately that $\epsilon_2 - \epsilon_1 > 0$ because of the electro-static energy cost of putting electrons in the middle layer. To determine t experimentally, it is only necessary to identify the gate voltage V_{13} at which inversion symmetry is established, and use Eq. (3.6). V_{13} may be determined in practice as the point where $(N_1 - N_2)$ is minimized, and electrostatic considerations give $V_{13} \approx V_3 + 4\pi e D_{FG}\bar{N}_2/\epsilon_0 \approx 0.1$ V, where $\bar{N}_2 \sim 6 \times 10^{10}$ cm^{-2} is the asymptotic value of N_2 at large V_{FG}. Unfortunately, the energy difference between E_1 and E_2 at the symmetric point is close to the limit of resolution of the experiment. An estimate of t can be obtained from the minimum difference between N_2 and N_3 (for $N_3 > 0$), which occurs when the densities of layers 1 and 2 are equal. This occurs at a front-gate voltage $V_{12} \approx V_3 + 4\pi e D_{FG}\bar{N}_3/\epsilon_0 \sim -0.1$ V, where $\bar{N}_3 \sim 3 \times 10^{10}$ cm^{-2} is the asymptotic value of N_3 at large V_{FG}. We obtain

$$t \approx \frac{1}{2} \min(E_3 - E_2) = \frac{\min(N_2 - N_3)}{2\nu_0} \approx 0.45 \quad \text{meV} \qquad (3.7)$$

for $(N_2 - N_3) \approx 2.5 \times 10^{10}$ cm^{-2}.

Subband densities can be extracted experimentally from weak-field SdH oscillation experiments. The parameters of the model (the offset voltages, the distances to the gates, the size-quantization energy ϵ_b, and the hopping parameter t) may be determined by fitting to the gate-voltage dependence of the measured subband densities. Experimental results are compared with a model fit in Fig. 2. The model calculations were performed with layer separation $d = 18.4$ nm, the mid-well to midwell distance in the experimental system. The offset voltages $V_{\alpha G}^{(0)}$ are consistent with the condition[18] that the electron density in the layers is left-right (LR) symmetric for $V_{FG} = 0.03$ V and $V_{BG} = 0$, when the total electron density is 14.8×10^{10} cm^{-2}. Close agreement with experiment is obtained by choosing the tunneling and on-site energies to be

within about 25% of $t = 0.4$ meV and 5% of $\epsilon_b = -4.6$ meV. The layer densities in Fig. 2 are in close agreement with the SdH data and with the layer densities obtained in Ref. 17 from 3D LDF calculations. This level of agreement provides us with the necessary confidence in our model, and determines with some assurance the model parameters for the system of immediate interest. We note that this calculation (for $B_\perp = 0$) explicitly neglects nonlocal interlayer exchange and correlation. This approximation appears to be well justified at zero magnetic field,[26] but we will see that in the strong magnetic-field limit, nonlocal interlayer exchange is important.

IV. QUANTUM HALL GROUND STATE

We now turn our attention to the strong magnetic-field limit. Reference 18 finds strong QHE's at $\nu_T = 1$ and 2; explaining the physics of the underlying incompressible states at these filling factors is the main objective of this paper. The fact that a QHE occurs at these integer filling factors is, at first sight, surprising. To understand why, it is useful to imagine repeating the calculations outlined in the previous section for $\nu_T = 1$. The crucial difference between the $B_\perp = 0$ and strong-field situations in such an independent-particle description is that, because the kinetic energy is quenched, the density of states consists of a δ function at the subband energies in the strong-field case, whereas it is a constant above the subband energy in the $B_\perp = 0$ case. As a result, the distribution of density between the three layers at $\nu = 1$, which we have emphasized is dictated largely by electrostatics, can be expressed simply in terms of the subband wave function:

$$n_j = (2\pi \ell^2)^{-1} |z_j^{(1)}|^2. \tag{4.1}$$

In order to have the charge distributed relatively equally among all the layers, the site energies cannot differ by more than $\sim t$. The difference between subband energies, which would give the QH activation gap in such a theory, would then also be $\sim t$. A gap of this size might be reduced or possibly eliminated by disorder in the samples. In the experiments, however, the observed gaps can be much larger than t. It seems clear that the explanation for these QHE's must lie in the interaction physics of the triple-layer system at strong fields, and that the gap would exist even if t were zero. Further evidence is found in the experimental observation that as the ratio of side-layer to middle-layer electron density is increased, the $\nu_T = 1$ state collapses, but the $\nu_T = 2$ state becomes stronger. We shall show that these observations are consistent with the behavior expected if spontaneous interlayer phase coherence occurs in these triple-layer systems. In the following, we focus on the case $\nu_T = 1$; the $\nu_T = 2$ case is simply related by a particle-hole transformation.[27] We shall also assume that the system has three layers, although most aspects generalize in an obvious way to systems with more than three layers.

The single Slater-determinant states considered in this section have the form

$$|\Psi\rangle = \prod_X^{N_\phi} \left(\sum_{j=1}^3 z_j \hat{c}_{jX}^\dagger \right) |0\rangle, \tag{4.2}$$

where z_j is the component in layer j of a normalized three-subband wave function, and $\hat{c}_{jX}^\dagger$ is the second-quantization operator that creates an electron in layer j, in the lowest Landau-level Landau-gauge state with guiding-center coordinate X. This wave function is a full Landau-level state for the subband with state vector $Z^\dagger = (z_1^*, z_2^*, z_3^*)$. In our HFA, we allow Z to be varied to minimize the energy. This variation generally results in a broken-symmetry ground state, since $z_i^* z_j \neq 0$ even when $t = 0$; i.e., the HF ground state has spontaneous interlayer phase coherence. For double-layer systems, the broken symmetry is robust under appropriate circumstances, and exists in the exact quantum-mechanical ground state. We expect spontaneous interlayer phase coherence to be similarly robust for triple-layer systems.

It is convenient to define the density matrix

$$\rho_{jk}(X) = \langle \Psi | \hat{c}_{jX}^\dagger \hat{c}_{kX} | \Psi \rangle = z_j^* z_k, \tag{4.3}$$

where $|\Psi\rangle$ is the coherent ground-state wave function, Eq. (4.2). Note that the filling factor of layer j is $\nu_j = \rho_{jj}$. In terms of the density matrix, the HF total energy is

$$E_{HF} = \sum_{jX} \left\{ -\sum_k t_{jk} \rho_{jk}(X) + \epsilon_j \rho_{jj}(X) \right.$$
$$- \sum_{\alpha Y} \bar{\nu}_\alpha D_{\alpha j}(Y) \rho_{jj}(X)$$
$$+ \frac{1}{2} \sum_{kY} [D_{jk}(X-Y) \rho_{kk}(Y) \rho_{jj}(X)$$
$$\left. - E_{jk}(X-Y) \rho_{kj}(Y) \rho_{jk}(X)] \right\}, \tag{4.4}$$

where t_{jk} denotes the tunneling energy between layers j and k, ϵ_j is the on-site size-quantization energy of layer j, and α indexes neutralizing planes of charges with areal charge density $ep_\alpha = e\bar{\nu}_\alpha/2\pi\ell^2$ produced by remote ionized donors or gates. The unit of length is the magnetic length, $\ell = \sqrt{\hbar c/eB}$. As an aside, we note that in the long-wavelength limit, E_{HF} has the form of a CP_{N-1} model[8] when expressed in terms of the z_j.[28]

In the lowest Landau level, the Coulomb interaction between electrons in layers j and k enters through the direct term $D_{jk}(X-Y)$ and the exchange term $E_{jk}(X-Y)$. These quantities are conveniently expressed in terms of projected Fourier transforms: e.g.,

$$D_{jk}(X) = \int \frac{d^2q}{(2\pi)^2} D_{jk}(q) e^{(1/4)q^2\ell^2} \int d^2r \langle X|r\rangle e^{iq\cdot r} \langle r|X\rangle, \tag{4.5}$$

where

$$D_{jk}(q) = \frac{2\pi e^2}{q} e^{-qd|j-k|} e^{-(1/2)q^2\ell^2}, \tag{4.6}$$

and

$$E_{jk}(q) = \frac{\ell^2}{2\pi} \int d^2p \, D_{jk}(p) e^{i(\hat{z}\cdot p\times q)\ell^2}. \tag{4.7}$$

The layers are located at $z = dj$, where j is in general a real number, unless all the layers are separated by integer multiples of d. We have neglected the finite thickness of the electron wave functions in the z direction, although this effect could be included, if desired.

When $\nu_T = 1$, it follows from Eq. (4.2) that

$$\rho_{jk}(X)\rho_{kj}(X) = \rho_{jj}(X)\rho_{kk}(X). \tag{4.8}$$

This relation, which follows from the phase-coherent nature of the assumed ground state, is of great practical importance to us, because unlike in the $B_\perp = 0$ case, it allows us to easily express the exchange contribution to the HF ground-state energy E_{HF}^0 in terms of the layer occupancies:

$$\frac{E_{\mathrm{HF}}^0}{N_\phi} = \sum_{jk} \left[-t_{jk}\sqrt{\nu_j\nu_k} + \delta_{jk}\left(\epsilon_j - \sum_\alpha \bar{\nu}_\alpha \bar{D}_{\alpha j} \right) \nu_j \right.$$
$$\left. + \frac{1}{2}(\bar{D}_{jk} - \bar{E}_{jk})\nu_j\nu_k \right], \tag{4.9}$$

where

$$\bar{D}_{jk} = -[D_0(q=0) - D_{|j-k|}(q=0)]/2\pi\ell^2 = -v_c\frac{d}{\ell}|j-k| \tag{4.10}$$

with $v_c \equiv e^2/\epsilon_0\ell$, and

$$\bar{E}_{|j-k|} \equiv \sum_X E_{jk}(X)$$
$$= \frac{E_{jk}(q=0)}{2\pi\ell^2}$$
$$= v_c\int_0^\infty dx\, e^{-(1/2)x^2}e^{-x|j-k|d/\ell}. \tag{4.11}$$

Equation (4.8) also allows us to write

$$\rho_{jk}(X) = \sqrt{\nu_j\nu_k}\,e^{i\phi_{jk}(X)}. \tag{4.12}$$

In the ground state, ρ_{jk} is independent of X, so that we may take $e^{i\phi_j(X)} = 1$. Since $\Sigma_j\nu_j = 1$, the HF ground state is in general determined by two parameters. We will concentrate below on the situation where the triple-layer system is symmetric, i.e., $\bar{\nu}_F = \bar{\nu}_B$. Then the system has inversion symmetry around the middle well, $\nu_1 = \nu_3$, and the ground state is completely fixed by ν_2.

The layer occupancies can be calculated by minimizing Eq. (4.9); equivalently, the following simple argument may be used in the absence of tunneling. For ϵ_b sufficiently large, all electrons reside in the side layers, closest to the gates. Suppose that both side layers (1 and 3) are occupied, and imagine moving an electron from layer 1 to the middle layer (2). The energy gained by moving to the middle has three components: the on-site energy ϵ_b, the Hartree energy $\bar{D}_1[(\nu_1 + \nu_3) - (\bar{\nu}_F + \bar{\nu}_B)]$ due to the direct Coulomb interaction with the side layers and gates, and the exchange energy $-\bar{E}_1(\nu_1 + \nu_3)$ of the middle electron with the side layers. The energy lost by moving to the middle also has three contributions: the Hartree energy $\bar{D}_2(\nu_3 - \bar{\nu}_B)$ of a layer-1 electron with the electrons in layer 3 and the gates, the on-site

exchange energy $-\bar{E}_0\nu_1$ in layer 1, and the exchange energy $-\bar{E}_2\nu_3$ of an electron in layer 1 with those in layer 3. Specializing to the case of $\nu_T = 1$, and using $\bar{D}_2 = 2\bar{D}_1$, the energy cost to move an electron to the middle layer is seen to be

$$\Delta E = \epsilon_b + \bar{D}_1[(\nu_1 - \nu_3) - (\bar{\nu}_F - \bar{\nu}_B)]$$
$$+ (\bar{E}_0 - \bar{E}_1)\nu_1 - (\bar{E}_1 - \bar{E}_2)\nu_2. \tag{4.13}$$

The middle layer will be occupied when $\Delta E < 0$. For the case of equal side-layer densities, this happens when $\epsilon_b < \epsilon_b^{\max}$, where

$$\epsilon_b^{\max} = -\tfrac{1}{2}(\bar{E}_0 - 2\bar{E}_1 + \bar{E}_2). \tag{4.14}$$

A similar argument can be used to find the value $\epsilon_b^{\min}$ of the on-site energy below which all electrons reside in the middle layer:

$$\epsilon_b^{\min} = -(-\bar{D}_1 - \bar{E}_0 + \bar{E}_1). \tag{4.15}$$

Equations (4.14) and (4.15) show that near-neighbor interlayer exchange ($\bar{E}_1$) plays an essential role in increasing the size of the interval where all three layers are occupied and spontaneous triple-layer phase coherence occurs. The local density approximation for exchange, commonly used in electronic structure calculations, fails qualitatively for triple-layer (and double-layer) systems in the QH regime, because it does not include the effects of interlayer exchange, included here through $\bar{E}_j$ for $j > 0$. The on-site exchange ($\bar{E}_0$) favors maximizing the charge of individual layers, and $\bar{E}_2$ favors next-nearest neighbor occupancy. For $\epsilon_b^{\min} \leq \epsilon_b \leq \epsilon_b^{\max}$, the middle-well occupancy decreases linearly with ϵ_b, so that

$$\nu_2 = \left[\frac{\epsilon_b^{\max} - \epsilon_b}{\epsilon_b^{\max} - \epsilon_b^{\min}} \right]. \tag{4.16}$$

When $\nu_2 = 1$, all the electrons are in the middle well, and we have, in effect, a single-layer system. When $\nu_2 = 0$, all the electrons are shared between the outside layers, and we have a double-layer system. For $0 < \nu_2 < 1$, charge exists in all three layers and the HFA ground state has triple-layer coherence.

We may use the HF ground-state calculation of ν_2 in Eq. (4.16) to define a phase diagram in the space of model parameters in the absence of interlayer tunneling. For symmetric triple-layer systems, the state of the system is determined by the middle-well size-quantization energy ϵ_b in units of the Coulomb energy $v_c \sim 10$ meV, and by the interlayer spacing d in units of ℓ. We consider the limit $t/v_c \ll 1$, which according to our analysis of the SdH data is satisfied by the device studied in Ref. 18, and set $t = 0$. The region of stability of the triple-layer coherent state at $t = 0$ is bounded by the dotted and dashed (upper and lower) lines of Fig. 3(a). These two lines are defined by the equations $\nu_2 = 1$ and $\nu_2 = 0$. At fixed d, the system transforms with increasing $|\epsilon_b|$, first from a double-layer system to a triple-layer system, and finally to a single-layer system with all the charge in the middle layer. At fixed ϵ_b, these transformations occur in the opposite order with increasing d, as electrostatic consider-
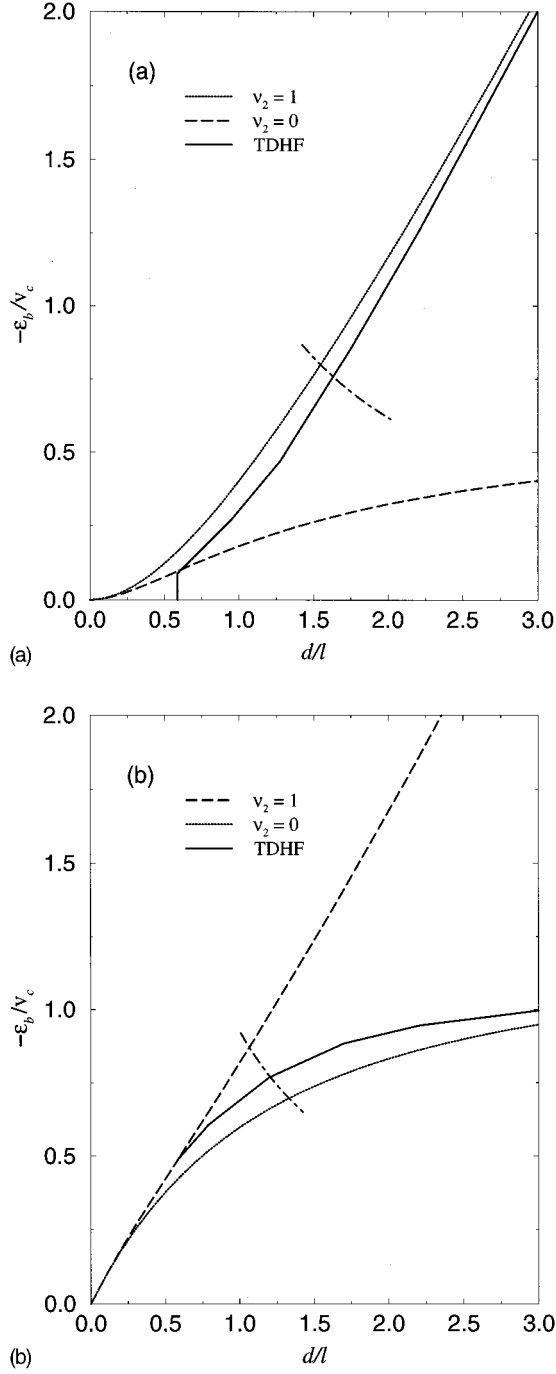
FIG. 3. (a) Phase diagram for the symmetric $\nu_T = 1$ 3LQH coherent state. (b) Phase diagram for the symmetric $\nu_T = 2$ 3LQH coherent state. The mean-field regions of stability lie between the dotted and solid lines. All calculations are for $t = 0$, for the case of equal left and right layer densities. The dot-dashed lines represent values of $(d/\ell, -\epsilon_b/v_c)$ obtained for a sample with $d = 18$nm, for total density in the range of 1 to 2×10^{11} cm^{-2}, using $\epsilon_b = -8$ meV for $\nu_T = 1$, and $\epsilon_b = -6$ meV for $\nu_T = 2$.

ations become more dominant. Figure 3(b) shows the same plot for $\nu_T = 2$, obtained from a calculation nearly identical to that of the $\nu_T = 1$ case. If, in a given sample, front and back gate voltages are adjusted simultaneously to maintain LR symmetry as the total density changes, the system will follow a line in this phase diagram that moves downward and toward the right with increasing magnetic field, as illustrated

in Fig. 3. By this procedure, the triple-layer regime should be accessible to experimental study in typical TLES's. The HF ground-state calculation by itself suggests that the entire region between the dotted and dashed lines in Fig. 3 might support a triple-layer coherent state. However, as we show in the following section, a stability analysis using the TDHF equations shows that for sufficiently large interlayer spacing, the phase-coherent state cannot be the ground state.

In closing this section, we remark that the distribution of electrons between the three layers can be markedly different for the same gate voltages and sample parameters in the QH regime, as compared to the $B_\perp = 0$ case. Reference 18 found, using their 3D LDF calculations, that for their triple-layer sample at symmetry, with a total density of 14.8×10^{10} cm^{-2}, the ratio of the density of electrons in the middle layer to the total density was $\nu_2/\nu_T \approx 0.22$ when $B_\perp = 0$. The 2D tight-binding model of the previous section gives the same result. For the same model parameters, we find that in the $\nu_T = 1$ phase-coherent triple-layer QH (3LQH) state, $\nu_2/\nu_T \approx 0.27$, while for $\nu_T = 2$ we obtain $\nu_2/\nu_T \approx 0.09$. The low value of ν_2/ν_T for $\nu_T = 2$ is due to the fact that for inversion-symmetric triple-layer systems, the $\lambda = 2$ subband wave function has no weight in the middle layer. Thus $B_\perp$ can have a large effect on the ratio of layer densities.

V. TIME-DEPENDENT HARTREE-FOCK COLLECTIVE MODES

In the TDHF description of the collective behavior, the variational wave function for the ground and excited states of the system both have the HF form, Eq. (4.2), but the density matrix elements ρ_{jk} are allowed to have spatial and time dependence. In particular, the low-lying collective modes arise from slow long-wavelength variations of the phase differences $\phi_{jk}(X)$. In practice, there are several ways to implement the TDHF approximation: diagrammatically, by path-integral methods, or by various equation of motion (EOM) approaches. TDHF collective modes for a triple-layer system were calculated previously by Fertig[29] using a diagrammatic approach, for the unphysical case of equidistant, individually charge-neutral layers with periodic boundary conditions, i.e., with the tunneling and Coulomb energies between end layers taken to be the same as between neighboring layers. Here we briefly describe a calculation based on the EOM of the density matrix. For the sake of generality, we use the language of an N-layer system, although we will apply our results to the case $N = 3$.

Following Ref. 30, we define the projected density-matrix operator

$$\hat{\rho}_{jk}(\mathbf{q}) = e^{(1/4) q^2 \ell^2} \sum_{XY} \hat{c}_{jX}^{\dagger} \left[\int d^2r \langle X|\mathbf{r}\rangle e^{-i\mathbf{q}\cdot\mathbf{r}} \langle \mathbf{r}|Y\rangle \right] \hat{c}_{kY},$$

(5.1)

and the density-density response function

$$\chi_{jklm}(\mathbf{q},t) = \frac{1}{i}\langle T\hat{\rho}_{jk}(\mathbf{q},t)\hat{\rho}_{jk}(-\mathbf{q},0)\rangle,$$

(5.2)

where T denotes the time-ordering operator. The physical quantities of interest to us are a function of $q = |\mathbf{q}|$, due to the isotropy of the system. The HFA to χ is obtained from the EOM

$$i\hbar\,\partial_t\hat{\rho}_{jk}(\mathbf{q})=[\hat{\rho}_{jk}(\mathbf{q}),\hat{H}_{\mathrm{HF}}], \qquad (5.3)$$

where $\hat{H}_{\mathrm{HF}}$ is the HF Hamiltonian. The commutator is evaluated by use of the identity

$$[\hat{\rho}_{jk}(\mathbf{p}),\hat{\rho}_{lm}(\mathbf{q})]=\delta_{kl}\hat{\rho}_{jm}(\mathbf{p}+\mathbf{q})e^{i(\hat{\mathbf{z}}\cdot\mathbf{p}\times\mathbf{q})\ell^2}$$
$$-\delta_{mj}\hat{\rho}_{lk}(\mathbf{q}+\mathbf{p})e^{i(\hat{\mathbf{z}}\cdot\mathbf{q}\times\mathbf{p})\ell^2}. \qquad (5.4)$$

In the TDHFA, $\chi(q,\omega)$ is obtained from the HF $\chi^{(0)}$ by including the effects of the Coulomb interaction between a particle in layer j and a hole in layer k with total in-plane momentum q, within a generalized random-phase approximation. This results in a Dyson equation for χ in terms of the direct and exchange interaction between a particle and hole. In matrix notation,

$$\chi=\chi^{(0)}+\chi^{(0)}\frac{1}{\hbar}W\chi, \qquad (5.5)$$

where $W=H-X$ is the sum of the Hartree and Fock contributions to the particle-hole interaction, given by

$$H_{jklm}(q)=\delta_{jk}\delta_{lm}\frac{D_{jl}(q)}{2\pi\ell^2}, \qquad (5.6)$$

and

$$X_{jklm}(q)=\delta_{jm}\delta_{kl}\frac{E_{jl}(q)}{2\pi\ell^2}. \qquad (5.7)$$

Since the layer indices each have N possible values, Eq. (5.5) may be solved numerically by inverting an $N^2\times N^2$ matrix.

The collective modes are obtained from the poles of $\chi(q,\omega)$ that have nonzero residues. The results of a sample calculation for $(t=0,-\epsilon_b/v_c=0.75,\ d/\ell=1.6)$, which has $\nu_2=0.838$, are shown in Fig. 4. (The collective mode for $\nu_T=2$ can be obtained from that for $\nu_T=1$ by particle-hole conjugation, using $\nu_2\to1-\nu_2$.) As seen from Fig. 4, there are two collective modes, which correspond to linear superpositions of variations in $\phi_{12}(X)$ and $\phi_{23}(X)$. As the spacing d between the layers increases, one of the collective modes softens and eventually becomes unstable at a wave vector $q\sim\ell^{-1}$. This signals the onset of a charge-density wave instability in the HFA, on which we comment further below. The lack of an anticrossing repulsion at the point (away from $q=0$) where the two collective-mode frequencies are equal is a special feature of the assumed LR symmetry of the charge distribution in the TLES. When this symmetry is present, the collective modes are excitations from a subband state ($\lambda=1$) that has even parity to subband states that have even ($\lambda=2$) or odd ($\lambda=3$) parity. The opposite parity between the two final states provides a selection rule that prevents the two collective modes from mixing.

So far, we have focused on the case where the tunneling t_{jk} is negligible compared to the Coulomb interaction energy scale v_c, and can be set to zero. This results in gapless Goldstone modes, as shown, for example, in Fig. 4. (When $1<\nu_T<N-1$, gapped collective modes exist, even in the absence of tunneling.) The tunneling energy can be varied by changing the thickness of the barrier between the quantum wells. The $[U(1)]^{N-1}$ invariance associated with the freedom to choose the $N-1$ relative phases $\phi_{j,j+1}$ in each layer
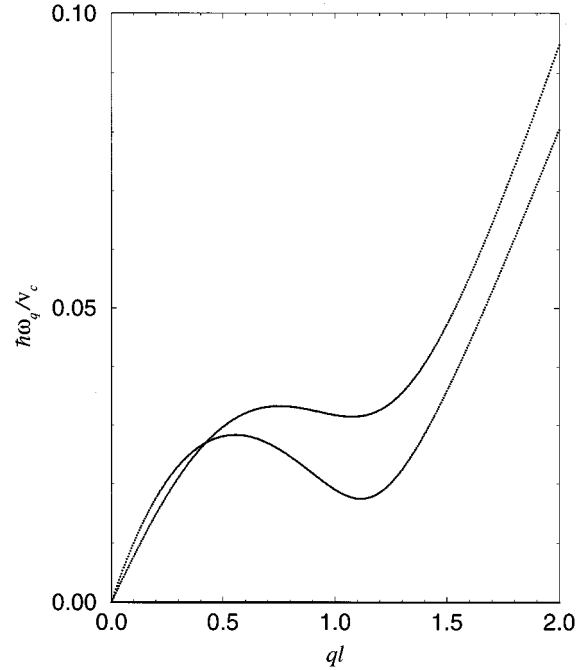

FIG. 4. Collective modes of the $\nu_T=1$ 3LQH coherent state for $(t=0,-\epsilon_b/v_c=0.75,\ d/\ell=1.6)$, which has $\nu_2=0.838$. The lack of an avoided crossing at $q\ell\sim0.4$ is due to the assumed left-right inversion symmetry of the system.

is broken once the electronic states in different layers are coupled by tunneling. The loss of this invariance gives a gap of order $2t$ (for nearest-neighbor $t_{jk}=t$) in the collective-mode spectrum as $q\to0$.

In our TDHF collective-mode calculations, we find that for fixed ϵ_b, the collective-mode spectrum in the triple-layer regime softens with increasing d, and that, except for sufficiently small values of d/ℓ, an instability occurs before the $\nu_2=0$ line in Fig. 3(a) is reached. The first collective mode that goes soft corresponds to an excitation from the filled $\lambda=1$ subband to the empty $\lambda=2$ subband, which has all the charge on the outside layers; this is the favored arrangement for the charge at large d. This instability appears in the TDHFA as an imaginary-valued collective-mode frequency. Based on extensive calculations performed previously for the case of double-layer systems,[30] the broken translational symmetry HF ground states that are found for larger values of d will quickly lose their interlayer phase coherence, and the charge gap (incompressibility) necessary for the integer QHE will rapidly go to zero. In our view, the broken translational symmetry of the state on the large-d side of this instability is likely to be an artifact of the HFA, which can enhance intralayer correlations only by breaking translational symmetry. When quantum fluctuations are included, the broken translational symmetry of this state is likely to be lost, but in our view the loss of interlayer phase coherence and the vanishing of the QH charge gap will remain. We therefore use the location of the TDHF instabilities as an estimate of the layer separation at which spontaneous coherence and the integer QHE are lost. The results are shown in Fig. 3(a) for $\nu_T=1$. The solid line shows the border of the TDHF instability. For $\nu_T=1$, the region between the upper dotted line ($\nu_2=1$)

where the middle layer is fully occupied, and the solid line, where the TDHF instability occurs, is the resulting estimate of the region in parameter space where a 3LQH coherent state occurs. This shows that as d/ℓ increases, the $\nu_T=1$ phase-coherent 3LQH state is more likely to be stable when the middle layer has *more* electrons than the side layers.[31] Figure 3(b) shows the phase diagram for $\nu_T=2$. In this case, the 3LQH state at larger d/ℓ is likely to be more stable when the middle layer has *fewer* electrons than the side layers. These behaviors are seen in the experiments of Ref. 18. The dot-dashed lines in Fig. 3 represent values of $(d/\ell, -\epsilon_b/v_c)$ for a hypothetical sample with $d=18$ nm, as the total density is varied from 1 to 2×10^{11} cm^{-2}, where we have used $\epsilon_b=-8$ meV for $\nu_T=1$ and $\epsilon_b=-6$ meV for $\nu_T=2$. As the total density and $B_\perp$ are increased while keeping the total filling factor ν_T constant, the dot-dashed lines in Fig. 3 show that the ratio of middle-layer density to side-layer density decreases. In all cases, the presence of interlayer tunneling will enlarge the region where a triple-layer QHE is expected to occur. We emphasize that the TDHF instability with increasing d is driven by the increasing relative importance of intralayer correlations compared to interlayer correlations. At large enough layer separations, the interlayer coherence that provides for good interlayer correlations will be lost, along with the charge gap necessary for the QHE. This scenario for the disappearance of the QHE with increasing layer separation does not require that the TLES make a transition to a bilayer system, as was hypothesized in Ref. 18.

VI. CONCLUDING REMARKS

We have shown that TLES's, such as those fabricated by Shayegan and co-workers, can be described using a simple tight-binding model, which allows them to be characterized in terms of a small number of parameters. The tight-binding model is able to quantitatively account for weak-field SdH experimental results for the dependence of the three subband energies on the gate voltage. Using this model, we have estimated the dependence of the ground state of the system on model parameters for filling factors $\nu_T=1$ and 2. We propose that in triple-layer systems, as in double-layer systems, the QHE can occur at integer total filling factors, even when the charge is distributed among all three layers and there is no hopping between the layers. (Tunneling would be required for noninteracting electrons to produce a gap at integer filling factors.) These QHE's occur because of the formation of broken-symmetry ground states with spontaneous interlayer coherence.

The distribution of charge between the three layers of the system is typically determined predominantly by electrostatic considerations, and states can occur with the electrons distributed among one, two, or three layers. Our HF theory of the ground state shows that for physically accessible regions of the middle-well on-site energy and layer separation, a triple-layer phase coherent state is possible. The stability of this state was estimated using the TDHFA, and a phase diagram was constructed, delimiting the regions in the parameter space of the TLES for which triple-layer coherence is likely to be found. The QH states studied by Shayegan and co-workers at $\nu_T=1$ and 2 show the behavior expected for phase-coherent states. In particular, they exhibit the QHE, even for small tunneling energies and unequal layer densities. Additionally, the $\nu_T=1$ QHE is suppressed by increasing occupancy of the side wells at the expense of the middle well, while for $\nu_T=2$, the opposite is true, in agreement with our findings. Future detailed comparisons between our phase diagram and experiment will be facilitated by the possibility of following lines in the phase diagram for a single sample, by adjusting gate voltages so that inversion-symmetric $\nu_T=1$ and 2 states occur for a range of magnetic fields. In any such quantitative comparison, it will be necessary to approximately account for the finite widths of the individual quantum wells, which we have not done here.

As in the case of the double-layer coherent state, a useful footprint of interlayer coherence is unusual sensitivity to small tilts of the magnetic field away from the normal to the layers.[15] The most convincing evidence for triple-layer coherence would be the observation of a strong suppression in the activation energy of the 3LQH states due to the application of a moderate parallel magnetic field. The state of the triple-layer system in a tilted magnetic field is most informatively described using a field-theoretical approach. We have calculated the magnitude of the parallel field required to suppress the activation energy as a function of the layer density, for both triple-layer and unbalanced double-layer systems. The effect of a parallel field on triple-layer states, charged order-parameter textures of triple-layer states, and other related properties of triple-layer phase-coherent states will be discussed in a forthcoming paper.[28]

[1] D. C. Tsui, H. L. Störmer, and A. C. Gossard, Phys. Rev. Lett. **48**, 1559 (1982).

[2] R. B. Laughlin, Phys. Rev. Lett. **50**, 1395 (1983).

[3] *The Quantum Hall Effect*, edited by R. E. Prange and S. M. Girvin (Springer-Verlag, Berlin, 1990).

[4] R. Tycko, S. E. Barrett, G. Dabbagh, L. N. Pfeiffer, and K. W.

West, Science **268**, 1460 (1995); S. E. Barrett, G. Dabbagh, L. N. Pfeiffer, K. W. West, and R. Tycko, Phys. Rev. Lett. **74**, 5112 (1995).

[5] E. H. Rezayi and F. D. M. Haldane, Bull. Am. Phys. Soc. **32**, 892 (1987)

[6] S. L. Sondhi, A. Karlhede, S. A. Kivelson, and E. H. Rezayi,

Phys. Rev. B **47**, 16 419 (1993).

[7] H. A. Fertig, L. Brey, R. Côté, and A. H. MacDonald, Phys. Rev. B **50**, 11 018 (1994).

[8] R. Rajaraman, *Solitons and Instantons* (North-Holland, Amsterdam, 1989).

[9] S. M. Girvin and A. H. MacDonald, in *Novel Quantum Liquids in Low-Dimensional Semiconductor Structures*, edited by S. Das Sarma and A. Pinczuk (Wiley, New York, 1995).

[10] X. G. Wen and A. Zee, Phys. Rev. Lett. **69**, 1811 (1992); Phys. Rev. B **47**, 2265 (1993).

[11] Z. F. Ezawa and A. Iwazaki, Int. J. Mod. Phys. B **19**, 3205 (1992); Phys. Rev. B **47**, 7295 (1993); **48**, 15 189 (1993).

[12] K. Yang, K. Moon, L. Zheng, A. H. MacDonald, S. M. Girvin, D. Yoshioka, and S. C. Zhang, Phys. Rev. Lett. **72**, 732 (1994).

[13] A. H. MacDonald, P. M. Platzmann, and G. S. Boebinger, Phys. Rev. Lett. **65**, 775 (1990); L. Brey, *ibid.* **65**, 903 (1990); O. Narikiyo and D. Yoshioka, J. Phys. Soc. Jpn. **62**, 1612 (1993); X. M. Chen and J. J. Quinn, Phys. Rev. B **45**, 11 054 (1992).

[14] J. P. Eisenstein, G. S. Boebinger, L. N. Pfeiffer, K. W. West, and S. He, Phys. Rev. Lett. **68**, 1383 (1992); Y. W. Suen, L. W. Engel, M. B. Santos, M. Shayegan, and D. C. Tsui, Phys. Rev. Lett. **68**, 1379 (1992).

[15] S. Q. Murphy, J. P. Eisenstein, G. S. Boebinger, L. N. Pfeiffer, and K. W. West, Phys. Rev. Lett. **72**, 728 (1994).

[16] J. Jo, Y. W. Suen, L. W. Engel, M. B. Santos, and M. Shayegan, Phys. Rev. B **46**, 9776 (1992).

[17] T. S. Lay, X. Ying, and M. Shayegan, Phys. Rev. B **52**, R5511 (1995).

[18] T. S. Lay, S. P. Shukla, J. Jo, X. Ying, and M. Shayegan, Surf. Sci. (to be published).

[19] A. H. MacDonald, Surf. Sci. **229**, 1 (1990).

[20] K. Moon, H. Mori, K. Yang, S. M. Girvin, A. H. MacDonald, L. Zheng, D. Yoshioka, and S. C. Zhang, Phys. Rev. B **51**, 5138 (1995).

[21] T. Ando, A. B. Fowler, and F. Stern, Rev. Mod. Phys. **54**, 437 (1982).

[22] M. Shayegan (private communication).

[23] W. Kohn and P. Vashishta, in *Theory of the Inhomogeneous Electron Gas*, edited by S. Lundqvist and N. H. March (Plenum, New York, 1983).

[24] J. P. Eisenstein, L. N. Pfeiffer, and K. W. West, Phys. Rev. Lett. **68**, 674 (1992); Phys. Rev. B **50**, 1760 (1994).

[25] For a discussion of the role of interlayer correlations in these experiments in the double-layer case, see T. Jungwirth and A. H. MacDonald, Phys. Rev. B **53**, 9943 (1996).

[26] Exchange-correlation effects on the effective interlayer tunneling parameter in double-layer systems are discussed by L. Świerkowski and A.H. MacDonald (unpublished).

[27] Spontaneous phase coherence can occur at nonintegral filling factors as well, but we restrict our attention here to the integer case where the mobility requirements for experimental systems are not as severe. This formalism also describes interlayer phase coherence in an N-layer sytem at filling factors $\nu_T = 1$ and $N-1$.

[28] C. B. Hanna and A. H. MacDonald (unpublished).

[29] H. Fertig, Phys. Rev. B **40**, 1087 (1989).

[30] R. Côté, L. Brey, and A. H. MacDonald, Phys. Rev. B **46**, 10 239 (1992).

[31] When $\epsilon_b \geq \epsilon_b^{max}$, so that only the two side layers are occupied, the TDHF instability occurs at $d_c/\ell = 0.589$, consistent with earlier TDHF calculations for double-layer systems (Refs. 13 and 29). We also find that d_c/ℓ *increases* when the charge densities of the two occupied layers are unequal (Ref. 28).